AN ONSET TO WHOLE BUILDING HYGROTHERMAL MODELLING UNDER WIND-DRIVEN RAIN LOADS

Masaru Abuku[1], Hans Janssen[2], and Staf Roels[1]

[1]Laboratory of Building Physics, Department of Civil Engineering, Katholieke Universiteit Leuven, Heverlee, Belgium

[2]Department of Civil Engineering, Technical University of Denmark, Lyngby, Denmark

ABSTRACT

This paper gives an onset to whole building hygrothermal modelling of the interaction between interior and exterior climates via building enclosures, which even takes into account wind-driven rain (WDR). First, the temporal and spatial distribution of WDR on the facades of a single leaf brick wall building is numerically determined. Then the hygrothermal behaviour of the walls and the room zone is numerically analysed. The results show that WDR loads can have significant impacts on the indoor climate, energy consumption and mould growth risk.

INTRODUCTION

Since the 1970s Building Energy Simulation (BES) models have been developed for the numerical prediction of the thermal condition and energy performance of a building. Though most BES models nowadays also (partially) solve the hygric balance, moisture analysis is mainly limited to water vapour transport and its influence through latent heat effects and moisture buffering. The comprehensive hygrothermal interaction between the exterior and interior climates, as dealt with in building envelope models (e.g. Pedersen, 1990; Künzel, 1994; Grunewald, 1997), is only incorporated to a limited extent. Recently, Nakhi (1995), Holm et al. (2003) and Rode et al. (2003) have combined a model of heat, vapour and liquid transport in walls with a BES model, to come to whole building hygrothermal modelling. This paper furthermore incorporates wind-driven rain (WDR) into such numerical simulation and focuses on liquid water transport.

Concerning WDR as boundary condition for the hygrothermal analysis of building envelopes, a lot of progress has been made in the last decades. Advanced numerical techniques based on Computational Fluid Dynamics (CFD) enabled the accurate numerical prediction of WDR loads on building facades (Choi, 1993; Blocken and Carmeliet, 2002). However, several topics related to the response of a wall to the driving rain load still need further investigation. Examples are durability issues of building facades, algae formation at exterior surfaces, the possible impact on mould growth at inside wall surfaces, and the impact on indoor climate and energy consumption. The answers to these questions do not only depend on the composition of the wall and the outside climate, but also on the building configuration, moisture buffering capacity of the interior, heat and moisture sources in the building, ventilation rate, etc. Such multicausal problems cannot be adequately dealt with via a component hygrothermal model, but do require whole building hygrothermal simulation.

Some of these interactions/dependencies are not of great concern for recent wall configurations, such as well-insulated walls with air cavity, walls with impermeable siding or sheathing, etc. On the other hand, in historic buildings in Europe, solid masonry systems have often been used for outer walls, without the installation of an adequate air space, insulation and/or vapour retarder, resulting in a direct capillary transmission between exterior and interior. For such walls, absorption of WDR loads may result in a moisture flow towards the interior surface and/or environment, potentially yielding mould growth at inside wall surfaces and/or increased indoor humidity. Hall and Kalimeris (1982) is perhaps the first case in which the impact of WDR loads on the moisture content in walls is investigated numerically. Janssen et al. (2007a, 2007b) and Blocken et al. (2007) first formulated the implementation of numerically determined WDR loads as boundary condition in the heat and moisture transfer analysis in building enclosures. Also Häupl et al. (2005) numerically investigated the impact of the rain on the hygrothermal performance of the facade of the 'Rijksmuseum' in Amsterdam, the Netherlands. Kumaraperumal et al. (2006) recently showed an experimental and numerical analysis of WDR loads on and the hygric response of the walls for a Scottish castle. Although the distribution of WDR load, with an intensity often highest near the upper edges and the sides of building facades, is considered to have an important role in the hygrothermal performance of buildings, so far no quantitative investigation of the impact of such distributed WDR load has been performed on a whole building scale. Neither has WDR been studied in relation to the durability, indoor environment and energy performance of a building. This paper presents an onset of such a study: the impact of the distributed WDR loads on

the hygrothermal behaviour of the walls and the indoor environment of a single leaf brick wall building has been investigated. In the first part of this paper, the methodology of the whole building simulation is briefly presented. In the second part, the WDR load on the facade of a $4 \times 4 \times 10$ m^3 tower is numerically determined. Then the heat and moisture transfer in the brick walls and the hygrothermal conditions in the room are numerically analysed on a horizontal slice through the walls at half the tower height. Finally the impact of WDR on the indoor climate, energy consumption and mould growth risk is discussed.

METHODOLOGY

In this paper a whole building simulation is defined as the numerical simulation of coupled heat, air and moisture transfer in building components and interior environment in rooms, with the aim of investigating the durability of building facades, together with an analysis of indoor climate and energy consumption of the building. When "perfect mixing" of indoor air is assumed, the whole building modelling of the interactions between exterior and interior climates via building components usually comprises: (1) the heat, air and moisture balance of the indoor environment; (2) the heat, air and moisture transfer in building components; and (3) the boundary conditions for (1) and (2) and the coupling of (1) and (2). Because essential parts of the whole building simulation are widely known and used in this field and only simple case studies are presented in this paper, the reader is referred to e.g. Nakhi (1995), Holm et al. (2003) and Rode et al. (2003) for a mathematical formulation of the whole building simulation. Note that the air transfer in porous building components has neither been considered in these whole building simulation models nor will be dealt with in the current study.

Whole building heat and moisture transfer

In the current study, the heat and moisture balances for the zone are expressed as

$$\rho_i c_i V \frac{\partial T_i}{\partial t} = Q_{wall} + Q_{vent} + Q_{internal} \qquad (1)$$

$$\rho_i V_i \frac{\partial X_i}{\partial t} = W_{wall} + W_{vent} \qquad (2)$$

where ρ_i is the density of the indoor air (kg/m^3), c_i is the specific heat of the indoor air (J/kgK), V is the volume of the room (m^3), t is the time (s), T_i is the temperature of the indoor air (K), X_i is the humidity ratio of the indoor air (kg/kg), Q_{wall} and W_{wall} are respectively the heat and moisture gain/loss (W and kg/s) at the entire interior wall surface, Q_{vent} and W_{vent} are respectively the heat and moisture gain/loss (W and kg/s) due to ventilation, $Q_{internal}$ is the internal heat gain/loss (W).

Also, the heat and moisture transfer equations in building components are expressed (e.g. Janssen et al. 2007a, 2007b) as:

$$c_{hh} \frac{\partial T}{\partial t} + c_{hm} \frac{\partial p_c}{\partial t} = \nabla(k_{hh} \nabla T + k_{hm} \nabla p_c) \qquad (3)$$

$$c_{mh} \frac{\partial T}{\partial t} + c_{mm} \frac{\partial p_c}{\partial t} = \nabla(k_{mh} \nabla T + k_{mm} \nabla p_c) \qquad (4)$$

where p_c and T are capillary pressure (Pa) and temperature (K) respectively, c_{hh} (J/m3K) and c_{hm} (J/m^{3}Pa) are the heat storage coefficients, c_{mm} (kg/m^{3}Pa) and c_{mh} (kg/m^{3}K) are the moisture storage coefficients, k_{hh} (W/mK) and k_{hm} (W/mPa) are the thermal conductivity due to the T-gradient and the p_c-gradient respectively, and k_{mm} (s) and k_{mh} (kg/msK) are the moisture permeability due to gradients in p_c and T respectively. Note that the air transfer in building components has hardly been considered in previous onsets of whole building simulation models and will also not be dealt with in the current study.

Boundary conditions at wall surfaces

The heat and moisture transfers in building components are coupled with the heat and moisture balances for the building zone by boundary conditions for heat and moisture exchange at inside wall surfaces of the zones, commonly using heat and moisture transfer coefficients. Thus the moisture and heat fluxes $g_{m,i}$ and $g_{h,i}$ at the inside wall surface are expressed as:

$$g_{m,i} = \beta_i(p_{v,i} - p_{v,s,i}) \qquad (5)$$

$$g_{h,i} = \alpha_{t,i}(T_i - T_{s,i}) + \beta_i(c_v T_{s,i} + L_v)(p_{v,i} - p_{v,s,i}) \qquad (6)$$

Here, β_i (s/m) is the moisture transfer coefficient at the inside wall surface; p_i and $p_{s,i}$ (Pa) are the vapour pressure of the indoor air and at the inside wall surface respectively; $\alpha_{t,i}$ (W/m^{2}K) is the total heat transfer coefficient at the inside wall surface; T_i and $T_{s,i}$ (K) are the temperature of the indoor air and at the inside wall surface; c_v (J/kgK) is the specific heat of the vapour water; and L_v (J/kg) is the heat of vaporisation.

Similarly, the heat and moisture transfer equations in building components require boundary conditions at the exterior side: outdoor air temperature and humidity, cloudiness, solar and diffuse radiation, convective heat and moisture transfer coefficient, and wind-driven rain intensity. Without splashing, bouncing, runoff of rain at building facades, the moisture flux at the outside wall surface $g_{m,e}$ (kg/m^{2}s) as boundary condition of the heat and moisture transfer equations in building components can be expressed as (e.g. Janssen et al. 2007a, 2007b):

$$g_{m,e} = \beta_e(p_{v,e} - p_{v,s,e}) + I_{WDR} \qquad (7)$$

Here, β_e (s/m) is the moisture transfer coefficient at the outside wall surface; p_e and $p_{s,e}$ (Pa) are the vapour pressure of the outdoor air and at the outside wall surface respectively; and I_{WDR} (kg/m^{2}s) is the WDR load. Note the assumption that the WDR load I_{WDR} is temporally averaged over a certain period (usually one hour).

The heat flux at the outside wall surface $g_{h,e}$ (W/m^2) that takes into account the WDR enthalpy can be expressed as:

$$g_{h,e} = R_s + R_1 + \alpha_{c,e}\left(T_e - T_{s,e}\right) \\ + \beta_e\left(c_v T_{s,e} + L_v\right)\left(p_{v,e} - p_{v,s,e}\right) + c_1 T_{WDR} I_{WDR} \quad (8)$$

Here, $\alpha_{c,e}$ (W/m^{2}K) is the convective heat transfer coefficient at the outside wall surface; T_e and $T_{s,e}$ (K) are the temperature of the outdoor air and at the outside wall surface; S_e (W/m^2) is the heat flux due to radiative heat exchange between the surface position considered and all the surroundings; c_1 (J/kgK) is the specific heat of the liquid water; and T_{WDR} is the temperature of WDR, which is assumed equal to T_e in the simulations of this paper.

When the wall surface is saturated and moisture is still supplied, the boundary condition can be given by the following equation instead of Equation (7).

$$p_c = 0 \quad (9)$$

Similarly, g_h is also expressed by the following equations instead of Equation (8):

$$g_{h,e} = R_s + R_1 + \alpha_{c,e}\left(T_e - T_{s,e}\right) \\ + \beta_e\left(c_v T_{s,e} + L_v\right)\left(p_{v,e} - p_{v,s,e}\right) + c_1 T_{WDR}\left(I_{WDR} - g_{ex}\right) \quad (10)$$

Here, g_{ex} (kg/m^{2}s) is the runoff of the excess water at the outside wall surface due to both WDR loads and/or surface condensation. The excess water is ignored for the remainder of the simulation.

The WDR load I_{WDR} (kg/m^{2}s) at building facades can be obtained by multiplying the horizontal rainfall intensity I_h (kg/m^{2}s) by the global catch ratio η (-) (Blocken and Carmeliet, 2002):

$$I_{WDR} = I_h \times \eta\left(\theta, U_{ref}, I_h\right) \quad (11)$$

where, η is a function of the angle θ (°) between reference wind direction and orientation of the wall, reference wind speed U_{ref} (m/s) and I_h, all obtained from meteorological data. η can be obtained from measurements (e.g. Sanders, 1996), empirical relations (Sanders, 1996) or numerical simulations (Choi, 1993; Blocken and Carmeliet, 2002). Note that detailed values of η can only be obtained by numerical simulation in a practical sense. For the methodology and a detailed discussion of the accuracy of such numerically determined catch ratio's the reader is referred to Blocken and Carmeliet (2002). The difference between determined WDR load and the actual moisture load

on the surface, due to the splashing and bouncing of raindrops, is discussed in Abuku et al. (2009), based on numerical and experimental investigations.

The numerical simulation of WDR as a source of moisture and enthalpy for a vertical wall is typically conducted assuming the WDR load spatially continuous and temporally averaged over a certain period. For the mathematical basis, the reader is referred to Janssen et al. (2007a).

CALCULATION STEPS AND BUILDING CONFIGURATION UNDER STUDY

The current study focuses on the hygrothermal response of a 4 m × 4 m × 10 m tower with brick walls of 29 cm thickness taking into account the WDR load on the facades. Figure 1 shows the configuration of the tower. Although the dimension of 4 m × 4 m × 10 m is rather small as building scale, this was adopted due to limits in computer capacity. WDR loads on the facades of this tower are first numerically determined by Computational Fluid Dynamics (CFD) and particle tracking simulations (Choi, 1993; Blocken and Carmeliet, 2002). As a second step, the hygrothermal response of the first floor (3.5 to 6.5 m above the ground) is analysed. Because of limits in computer capacity, the analysis is performed on a 2-dimensional horizontal slice of the walls and the room (4 m × 4 m). Thus it is assumed that the rain load on this part is vertically uniform and hence that the vertical distribution of heat and moisture in the walls of this part is also uniform. WDR loads are vertically averaged to obtain representative WDR loads for vertical segments from 3.5 to 6.5 m above the ground. In the current study the masonry is treated as homogeneous, while in reality masonry consist of brick and mortar, which may change the penetration rate of rain into the wall and thus have some influence on results in section 5.
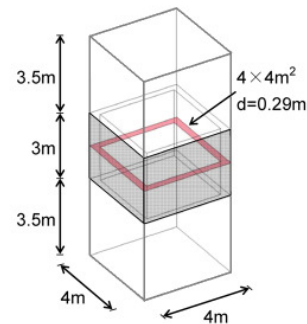

Figure 1 Configuration of the building and section under study. d: thickness of the wall (m).

NUMERICAL QUANTIFICATION OF WDR LOADS

The WDR for the facades of the 4×4×10 m3 tower was calculated with the method of Blocken and

Carmeliet (2002). As a first step, the simulation of the airflow field was performed by CFD. The detailed condition of this CFD simulation is described in Abuku et al. (2009). Secondly, the trajectories of raindrops with a diameter of 0.3, 0.4, 0.5, 0.6, 0.7, 0.8, 0.9, 1.0, 1.2, 1.4, 1.6, 1.8, 2.0, 3.0, 4.0, 5.0 and 6.0 mm were simulated for 5 reference wind speeds (2, 4, 6, 8 and 10 m/s). Then the specific catch ratio was calculated based on the trajectory of raindrops, and the specific catch ratio data were integrated into the global catch ratio. The catch ratio η for a wind perpendicular to the facade was vertically averaged from 3.5 to 6.5 m above the ground. When the wind is oblique to the facade, the cosine projection method was adopted for the calculation of the catch ratio based on Janssen et al. (2007b).

Finally, WDR intensities at the exterior wall surfaces with an interval of 0.2 m were calculated for the climate conditions of Essen of Germany, using the catch ratio data determined above, depending on wind speed, wind direction, horizontal rainfall intensity, and orientation of the building facades. The time course of their cumulative amounts over the year at the edges and the centres of the walls is shown in Figure 2. Due to the prevailing SW wind direction in Essen, the WDR load is concentrated at the west-facing facade and some WDR is loaded onto the north- and south-facing facades, while almost no WDR reaches the east-facing facade. For each facade, the WDR load is the highest at the edges of the wall and the lowest at the centre of the wall.

NUMERICAL ASSESSMENT OF WDR IMPACTS ON BUILDINGS

Condition of numerical analyses

In this section, three simulations are conducted: (1) the interior relative humidity over the year was calculated taking into account a constant ventilation rate of 0.5 ACH and a constant indoor temperature of 20 °C, but not linked to heat and moisture transfer through the walls; (2) in addition to the conditions of (1), the evaporation and absorption at the outside and inside wall surfaces were taken into account but WDR loads at the outside wall surfaces were neglected; (3), in addition to the conditions of (2) the WDR were loaded onto the outside wall surfaces. Case (1) purely shows the ventilation effects on the heat and moisture balance in the room. The comparison of case (1) and (2) shows the importance of the hygric inertia. The comparison of case (2) and (3) shows the WDR impact.

Numerical simulations were carried out with the 2-dimensional horizontal slice of the brick walls (4 m × 4 m) and the room. The room temperature and humidity was assumed spatially uniform in the room, employing the "perfect mixing" assumption, and was calculated in all three cases. The heat and moisture

transfer in the horizontal slice of the brick walls was analysed in case (2) and (3) with the FEM method (Janssen, 2007a) under the following conditions.

Equations (1) and (2) and Equations (3) and (4) are coupled by Equations (5) and (6) respectively. The exterior boundary conditions of Equations (3) and (4)
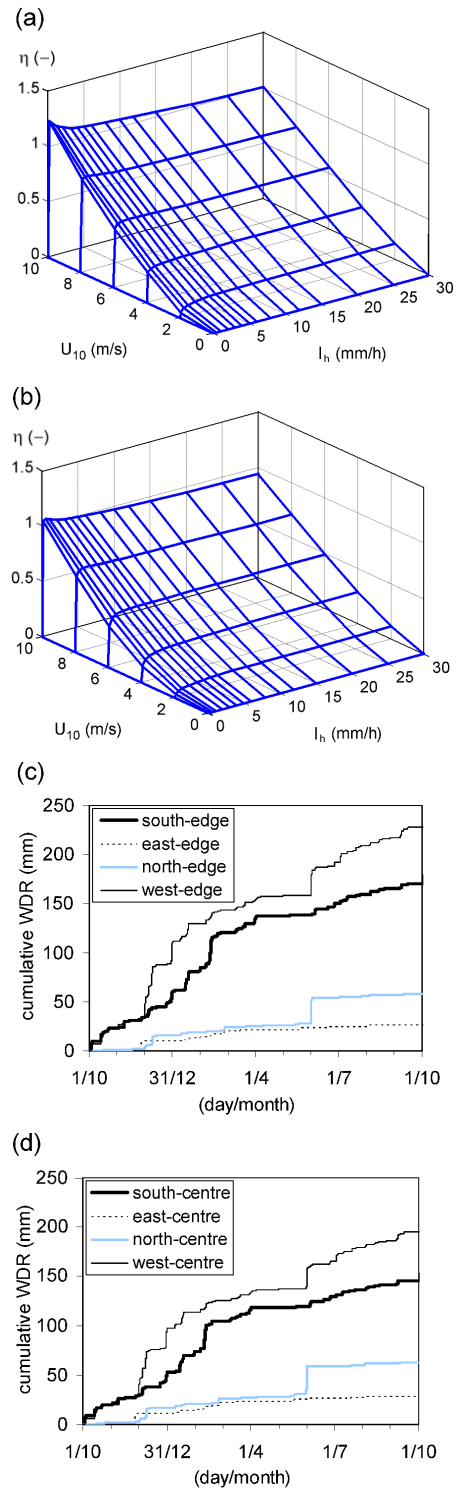
Figure 2 (a,b) Catch ratio η and (c,d) cumulative wind-driven rain (WDR) vertically averaged from 3.5 to 6.5 m above the ground at (a,c) the edges and (b,d) the centres on the facades.

are given by Equations (7-10). Equations (1) and (2) for the calculation of the room zone are solved explicitly, whereas the FEM code by Janssen et al. uses a fully implicit scheme. In each time step, the calculation is performed in two successive steps as illustrated in Figure 3: (1) the temperatures and moisture contents in the walls and the heat and moisture fluxes at the wall surfaces at the new time step (t+Δt) are calculated, based on the (constant) indoor air temperature (independent of time), the indoor relative humidity and the temperatures and moisture contents in the walls at the previous time step (t), and the meteorological data at the new time step (t+Δt); (2) the energy consumption and indoor relative humidity of the room at the new time step (t+Δt) are calculated, based on the (constant) indoor air temperature (independent of time), the indoor relative humidity at the previous time step (t), and the heat and moisture fluxes at the (interior) wall surfaces and the meteorological data at the new time step (t+Δt). Note that Δt is limited to 600 seconds to avoid numerical errors.
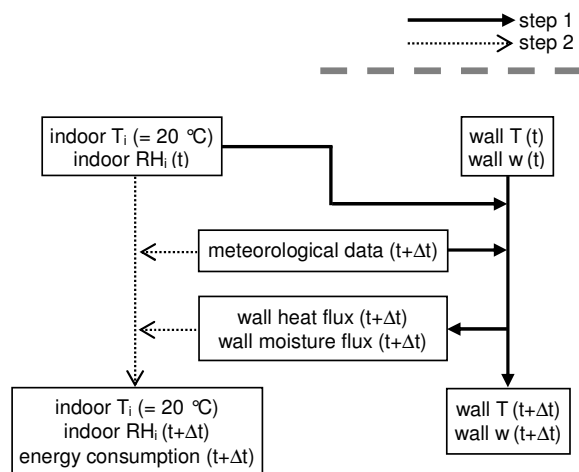

Figure 3 Two successive steps to calculate (step 1) the temperatures (T) and moisture contents (w) in the walls and the heat and moisture fluxes at the wall surfaces and (step 2) the energy consumption and indoor relative humidity (RH$_i$) of the room. Ti: (constant) indoor air temperature (= 20 °C); t: the previous time step; t+Δt: the new time step.

The horizontal slice of the walls was discretised with 18000 linear triangular elements (18360 nodes). 51 nodes were assigned for an intersection of the walls. The material properties of brick were taken from the benchmark 'Response analysis' of the European project HAMSTAD (Hagentoft et al., 2004). Note that short wave absorptivity and long-wave emissivity of brick were taken as 0.5 and 0.9 respectively. In the current study, a yearly climate data record of Essen of Germany was used. The cloudiness was kept constant at 0.6. The WDR loads calculated in the previous chapter (the data at the edges and centres of the facades are given in Figure

2) were used in the current simulation. Note that the catch ratios for the positions of the nodes at the exterior wall surfaces were calculated by a linear interpolation of the given values for the two neighbouring positions which are given with an interval of 0.2 m.

Outside surface film coefficients were kept constant at 20 W/m²K for heat transfer and 1.54×10^{-7} s/m for moisture transfer. In reality, these values depend on wind speed, wind direction and position on the facade, and they may have a significant influence on the moisture response (Janssen et al., 2007b). However, because the exact spatial and temporal variation of the values is unknown, constant values (independent of space and time) were adopted in the current simulations. Inside surface film coefficients are based on the measurement results of IEA Annex 14 (Reiβ and Erhorn, 1991). The total inside surface film coefficient for heat transfer at a position x m away from the edge of the inside wall surface $\alpha_{ti}(x_i)$ (W/m²K) is expressed by:

$$\alpha_{t,i}(x_i) = \alpha_{t,i,centre}\left\{1-\left(1-\frac{\alpha_{t,i,edge}}{\alpha_{t,i,centre}}\right)\exp\left(-3\frac{x_i}{d}\right)\right\} \quad (12)$$

with $\alpha_{t,i,centre}$ the total heat transfer coefficient at the centre of the inside wall surfaces (W/m²K); $\alpha_{t,i,edge}$ the total heat transfer coefficient at the edges of the inside wall surfaces (W/m²K); d the wall thickness (m) (= 0.29 m). In the current simulations $\alpha_{t,i,centre}$ and $\alpha_{t,i,edge}$ are arbitrarily kept constant at 8 and 6 W/m²K respectively (Reiβ and Erhorn, 1991). The values in reality might be even smaller than these values (Reiβ and Erhorn, 1991), especially when e.g. furniture is placed against the wall or when the indoor air is extremely stagnant. The moisture transfer coefficient at the inside wall surfaces β$_i$ is determined from half the total heat transfer coefficient $\alpha_{t,i}(x_i)/2$ (to exclude the radiation effects), by use of the Lewis relation.

Figure 4 plots three spatially distributed conditions: the total heat transfer coefficient at the interior wall surfaces and the cumulative WDR and solar gain at the exterior wall surfaces over the year.

Finally, the initial temperature and RH in the walls are set at 20 ˚C and 50 % respectively and the initial indoor RH is set at 50 %.

Impact on indoor climate

In this part, the three simulations are compared to show influences of ventilation, moisture buffering effects of the walls and impacts of the WDR loads. The evolution with time of the indoor RH of the 3 cases over the year is shown in Figure 5. Comparing conditions. When the results with WDR load (case (3)) are compared to those without WDR load (case (2)), the seasonal impact of WDR on energy consumption under such conditions is estimated as
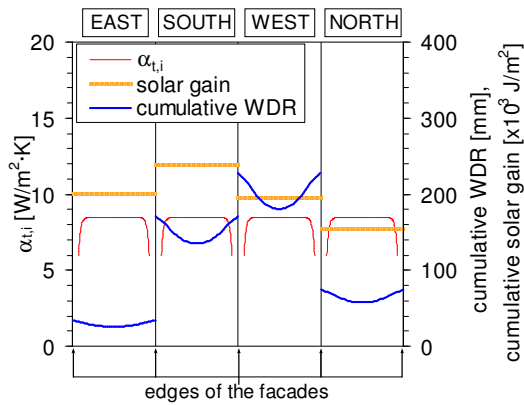
Figure 4 Spatial distribution of the total heat transfer coefficient at the interior wall surfaces, and the cumulative WDR and solar gain at the exterior wall surfaces over the year. The four sections represent the facades facing to east, south, west and north.

18.7 % in winter (December, January and February); 3.8 % in spring (March, April and May); 21.5 % in the simulation results without WDR load and those with only ventilation shows that the absorption and evaporation at the wall surfaces have a very small effect on indoor RH change (see Figure 5 (b)), which is attributable to the low buffering potential of the ceramic brick in the hygroscopic region. On the other hand, the comparison of the results with WDR load to those without WDR load shows that WDR load causes a significant increase of indoor relative humidity of up to 55 % under the conditions considered, which is seen at 7th of March. The differences between the results with WDR load and those without WDR load are significant in winter and summer due to increases of the moisture content at the inside wall surfaces; it is less significant in spring and autumn.
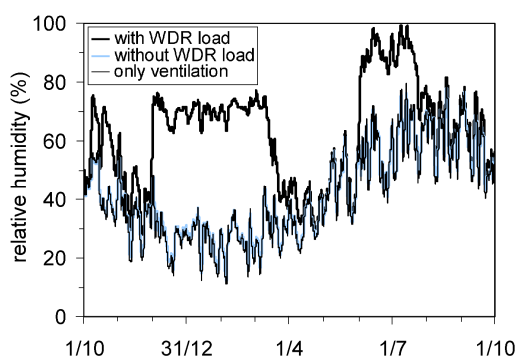

Figure 5 Time evolution of indoor relative humidity of the 3 cases over the year.

Impact on energy consumption

Seasonal energy consumptions are given in Table 1, comparing the results of the 3 cases. Comparing the results without WDR (case (2)) to those with only ventilation (case (1)) shows that the energy consumption is mainly influenced by the heat flow through the (uninsulated) walls and that ventilation is

less important for energy consumption in the current summer (June, July and August); and 4.4 % in autumn (September, October and November). The energy consumption for heating in summer is very low, though. Note that the current building configuration has no window, so that the impact on energy consumption in summer can be much smaller in reality due to the solar and diffuse radiations. The annual impact is estimated as 11.8 %. The impact of WDR is considered to be smaller when the ventilation rate is more important for energy consumption. Note that for hot climates the results may be different, since the energy consumption for cooling in summer periods may decrease through increased transmission losses to the outside due to rain loads (Hokoi, 1986), while the increased RH due to rain loads may still increase the latent cooling loads and a rain load may also increase the energy consumption for heating in winter.

Table 1
Seasonal and annual energy consumption.
(1) only ventilation; (2) ventilation + evaporation / absorption without WDR load; (3) ventilation + evaporation / absorption with WDR loads; (4) = ((3) - (2)) / (2) × 100 (impact of WDR).

	(1)	**(2)**	**(3)**	**(4)**
Winter	77.8 kWh	853 kWh	1013 kWh	18.7 %
Spring	50.0 kWh	516 kWh	536 kWh	3.8 %
Summer	20.3 kWh	165 kWh	201 kWh	21.5 %
Autumn	43.6 kWh	465 kWh	485 kWh	4.4 %
Annual	192 kWh	1999 kWh	2234 kWh	11.8 %

Impact on mould growth risk

One of the advantages of whole building simulations is the possibility of assessing the risk of mould growth at building wall surfaces. In this part, the simulation results without WDR load are compared with the one with the WDR load and the impact of the WDR load on mould growth at inside wall surfaces is discussed.

Figure 6 shows the daily averaged temperature and relative humidity at the edge (facing south-west) and centre (facing south) of the inside wall surfaces on the graphs of generalised isopleths of the spore germination time of the fungus mould for substrate category I (Sedlbauer, 2001). Figure 6 (a) and (b) show the results of the simulation without WDR load and Figure 6 (c) and (d) show the results with the WDR load. The same plots can be applied to the mycelium growth rate and similar conclusions can be drawn as shown below. Though brick is considered to be in the substrate category II, the isopleths for the substrate category I are adopted here as worst case scenario. If the relative humidity for a given temperature is below the line of ∞ days, no biological activity is expected. Note that, when the RH is too high (e.g. RH > at least 96 % (Sedlbauer, 2001)), the mould may not grow but can still exist.
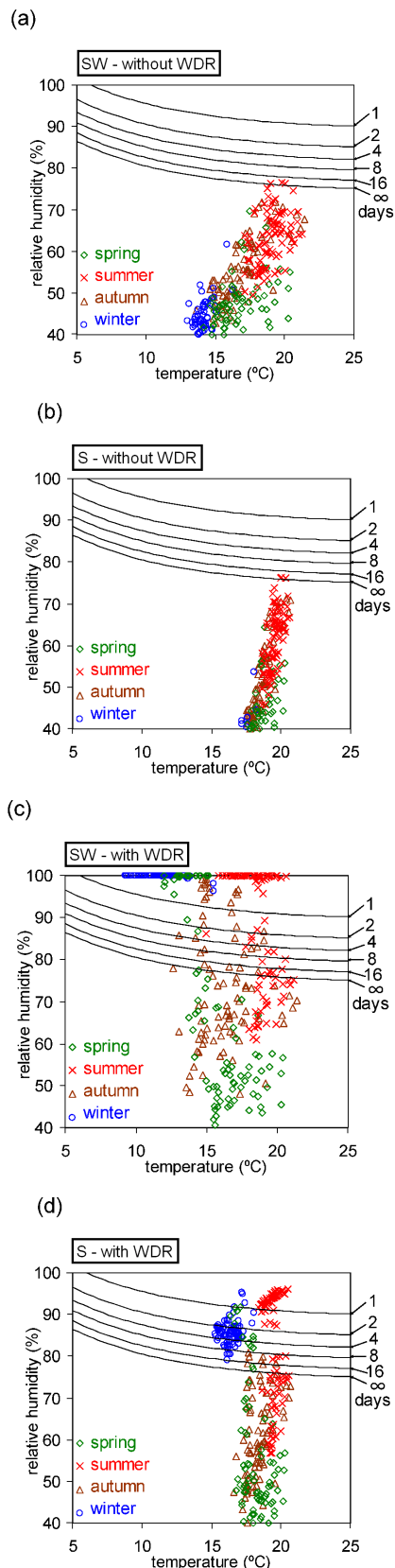
Figure 6 Daily averaged temperature and humidity at the inside wall surfaces on the graph of generalised isopleths of the spore germination time (black solid lines) of the fungus mould for the substrate category I. (a,c) SW facing edge; (b,d) S facing centre. (a,b) without WDR; (c,d) with WDR.

Each figure compares seasonal risks. Analysing the risk without taking into account WDR (see Figure 6 (a) and (b)), no mould growth is expected; but, when the WDR is taken into account, looking at Figure 6 (c) and (d), a serious risk on mould growth can be expected, mainly in summer and winter, with a more serious risk in summer than in winter. The comparison of the results of the simulation with WDR and those without WDR shows that the impact of WDR on the mould growth at the inside wall surfaces is significant.

Comparing Figure 6 (c) and Figure 6 (d), a wider variation of surface temperatures is seen at the edge than at the centre and the surface temperatures are averagely lower at the edge than at the centre. The reason of this difference is that the surface temperature at the edge is more influenced by the outdoor temperature, which can even result in a lower risk at the edge than at the centre. When the variations and criteria of temperature and relative humidity are considered together, it is concluded that, for the current case, the criterion of relative humidity for mould growth is more severe than that of temperature.

CONCLUSION

An onset was given to whole building modelling and simulations of the interaction between interior and exterior climates via building enclosures with emphasis on wind-driven rain (WDR). The impacts of WDR loads on the hygrothermal response of the walls, indoor climate, energy consumption and mould growth risk at the inside wall surfaces were investigated. The hygrothermal response of the solid brick walls and indoor climates of a cubic building with distributed WDR loads was numerically analysed. For the case analysed, the simulations showed that WDR causes a significant increase of indoor relative humidity and energy consumptions for heating. Furthermore the obtained relative humidity and temperature at the interior wall surfaces were combined with isopleths of generalised spore germination time of fungus mould. The results showed that WDR loads can have a significant impact on mould growth especially at the edge of the wall.

The results obtained here are considered to strongly depend on the material properties, climate, etc. Yet the climate and some of the historical buildings in Europe and some other countries are indeed not far from the conditions used for the current study. The results also indicated that similar investigation of WDR load impact even for different climates and other building wall materials, such as natural stone, can be worth the effort.

ACKNOWLEDGEMENT

REFERENCES

Abuku M., Janssen H., Poesen J. and Roels S. 2009. Impact, absorption and evaporation of raindrops on building facades, Building and Environment, 44(1), 113-124.

Blocken B. and Carmeliet J. 2002. Spatial and temporal distribution of wind-driven rain on low-rise building, Wind and Structure, 5(5), 441-462.

Blocken B., Roels S. and Carmeliet J. 2007. A combined CFD-HAM approach for wind-driven rain on building facades, Journal of Wind Engineering and Industrial Aerodynamics, 95(7), 585-607.

Choi E.C.C. 1993. Simulation of wind-driven-rain around a building, Journal of Wind Engineering and Industrial Aerodynamics, 46&47, 721-729.

Grunewald J. 1997. Diffusiver und konvektiver stoff- und energietransport in kapillarporösen baustoffen, PhD thesis, Dresden University of Technology.

Hagentoft C.-E., Kalagasidis A.S., Adl-Zarrabi B., Roels S., Carmeliet J., Hens H., Grune-wald J., Funk M., Becker R., Shamir D., Adan O., Brocken H., Kumaran K. and Djebbar R. 2004. Assessment method of numerical prediction models for combined heat, air and moisture transfer in building components: benchmarks for one-dimensional cases, Journal of thermal envelope and building science, 27(4), 327-352.

Hall C. and Lalimeris A.N. 1982. Water movement in porous building materials–V. Absorption and shedding of rain by building surfaces, Building and Environment, 19, 13-20.

Häupl P., Grunewald J. and Ruisinger U. 2005. Hygrothermal 2-dimensional analysis of critical constructive details of the Rijksmuseum Amsterdam, Report, Institute for Building Climatology, Dresden University of Technology, Germany.

Hokoi S. 1986. Fundamental study of thermal characteristics of wet building walls, PhD thesis, Kyoto University.

Holm A., Kunzel H., and Seldbauer K. 2003. The hygrothermal behaviour of rooms: combining thermal building simulation and hygrothermal envelope calculation, in: Proceedings of the Eighth International IBPSA Conference, Eindhoven, The Netherlands, August 11-14, 2003, 499-505.

Reiß J, Erhorn H. 1991. IEA Annex 14, Condensation and Energy, Final Report, Volume 1, Source Book, Leuven: Acco Uitgeverij, pp. 3.50-3.53.

Janssen H., Blocken B. and Carmeliet J. 2007a. Conservative modelling of the moisture and heat transfer in building components under atmospheric excitation, International Journal of Heat and Mass Transfer, 50, 1128-1140.

Janssen H., Blocken B., Roels S. and Carmeliet J. 2007b. Wind-driven rain as a boundary condition for HAM simulations: Analysis of simplified modelling approaches, Building and Environment, 42, 1555-1567.

Kumaraperumal A., Sanders C. and Baker P. 2006. CFD and hygrothermal modeling are compared with full-scale measurements to predict the fabric moisture contents due to wind-driven rain on a Scottish castle, International Report, IEA Annex 41, Task 3 - Boundary condition, A41-T3-UK-06-2.

Künzel H.M. 1994. Verfahren zur ein- und zweidimensionalen Berechnung des gekoppelten Wärme- und Feuchtetransports in Bauteilen mit einfachen Kennwerten, PhD thesis, University of Stuttgart.

Nakhi A.E. 1995. Adaptive construction modelling within whole building dynamic simulation. PhD thesis, University of Strathclyde.

Pedersen C.R. 1990. Combined heat and moisture transfer in building constructions, PhD thesis, Technical University of Denmark.

Rode C., Salonvaara M., Ojanen T., Simonson C. and Grau K. 2003. Integrated hygrothermal analysis of ecological buildings. in: Proceedings of the 2nd International Conference on Building Physics, Leuven, Belgium, September 14-18, 2003, 859-868.

Sanders C. 1996. Heat, air and moisture transfer in insulated envelope parts. IEA Annex 24, Final report – Vol. 2, Task 2: Environmental conditions, Acco Leuven, 75-85.

Sedlbauer K. 2001. Vorhersage von Schimmelpilzbildung auf und in Bauteilen (Predictuion of mould manifestation on and in building parts), PhD thesis, University of Stuttgart.